Published OnlineFirst May 9, 2014; DOI: 10.1158/1535-7163.MCT-13-0903

Small Molecule Therapeutics

Molecular Cancer Therapeutics

EW-7197, a Novel ALK-5 Kinase Inhibitor, Potently Inhibits Breast to Lung Metastasis

Ji Yeon Son[1], So-Yeon Park[1], Sol-Ji Kim[1], Seon Joo Lee[1], Sang-A. Park[1], Min-Jin Kim[1], Seung Won Kim[1], Dae-Kee Kim[1], Jeong-Seok Nam[2], and Yhun Yhong Sheen[1]

Abstract

Advanced tumors produce an excessive amount of transforming growth factor β (TGFβ), which promotes tumor progression at late stages of malignancy. The purpose of this study was to develop anti-TGFβ therapeutics for cancer. We synthesized a novel small-molecule TGFβ receptor I kinase (activin receptor–like kinase 5) inhibitor termed *N*-[[4-([1,2,4]triazolo[1,5-*a*]pyridin-6-yl)-5-(6-methylpyridin-2-yl)-1*H*-imidazol-2-yl]methyl]-2-fluoroaniline (EW-7197), and we investigated its potential antimetastatic efficacy in mouse mammary tumor virus (MMTV)/c-Neu mice and 4T1 orthotopic–grafted mice. EW-7197 inhibited Smad/TGFβ signaling, cell migration, invasion, and lung metastasis in MMTV/c-Neu mice and 4T1 orthotopic–grafted mice. EW-7197 also inhibited the epithelial-to-mesenchymal transition (EMT) in both TGFβ-treated breast cancer cells and 4T1 orthotopic–grafted mice. Furthermore, EW-7197 enhanced cytotoxic T lymphocyte activity in 4T1 orthotopic–grafted mice and increased the survival time of 4T1-Luc and 4T1 breast tumor–bearing mice. In summary, EW-7197 showed potent *in vivo* antimetastatic activity, indicating its potential for use as an anticancer therapy. *Mol Cancer Ther; 13(7); 1704–16. ©2014 AACR.*

Introduction

Transforming growth factor β (TGFβ) is a multifunctional cytokine that plays a central role in a variety of cellular processes, including cell growth, differentiation, cell adhesion, migration, and extracellular matrix deposition (1). The binding of TGFβ to a heteromeric complex containing the TGFβ receptor facilitates activation of activin receptor–like kinase 5 (ALK5), which phosphorylates Smad2/3 (2). Phosphorylated Smad2/3 then forms a heteromeric complex with Smad4 and is translocated into the nucleus (3), resulting in altered gene expression (4, 5). One of the main functions of TGFβ signaling is preservation of the homeostasis of epithelial, endothelial, and hematopoietic cells. However, in pathologic circumstances, the homeostatic action of TGFβ is diverted to alternative roles. During cancer progression, TGFβ signaling plays a dual role. At the early stages of tumorigenesis, TGFβ signaling elicits a preventive or tumor-suppressing effect, and epithelial cells retain delicate growth sensitivity to TGFβ. However, at later stages, when carcinoma cells become resistant to TGFβ-mediated growth inhibition, the intracellular signaling circuitry of cells is altered and leads to the progression of tumors (6). TGFβ ligands are often enriched in the breast tumor microenvironment and can be produced by tumor cells or tumor-associated stromal and immune cells (4, 7). In addition, TGFβ has been shown to play a critical role in breast cancer metastasis to the lung and in the maintenance of cancer stem cells (CSC) in breast carcinomas (8–11). TGFβ is also a potent inducer of the epithelial-to-mesenchymal transition (EMT) in mammary cells (12), and this transformation has been associated with the acquisition of tumor stem-like properties (13). Indeed, the TGFβ receptor I/II kinase inhibitor has been shown to reverse EMT and induce the mesenchymal-to-epithelial transition in $CD44^+$ mammary epithelial cells (7). Studies with triple-negative breast cancer cells further suggest that CSCs with self-renewing and tumor-initiating capacities are responsible for chemotherapy resistance and relapse after treatment (14). Therefore, inhibition of the TGFβ signaling pathway offers a rational approach to cancer therapy. Thus far, the following three approaches have been used to inhibit TGFβ signaling: (i) inhibition of TGFβ signaling at a translational level using antisense oligonucleotides (15, 16); (ii) inhibition of the ligand–receptor interaction using monoclonal antibodies (mAb; refs. 17–20); and (iii) inhibition of the receptor-mediated signaling cascade using inhibitors of TGFβ receptor kinases (21). Small-molecule inhibitors of TGFβ/ALK5

Authors' Affiliations: [1]College of Pharmacy, Ewha Womans University, Seodaemun-gu, Seoul; and [2]Laboratory of Tumor Suppressor, Lee Gil Ya Cancer and Diabetes Institute, Gachon University, Incheon, South Korea

Note: Supplementary data for this article are available at Molecular Cancer Therapeutics Online (http://mct.aacrjournals.org/).

J.Y. Son and S.-Y. Park contributed equally to this work.

Corresponding Authors: Yhun Yhong Sheen, College of Pharmacy, Ewha Womans University, Seodaemun-gu, Seoul, 120-750, South Korea. Phone: 82-2-3277-3028; Fax: 822-3277-2851; E-mail: yysheen@ewha.ac.kr; and Jeong-Seok Nam, Laboratory of Tumor Suppressor, Lee Gil Ya Cancer and Diabetes Institute, Gachon University, 7-45, Songdo-dong, Yeonsu-ku, Incheon, 406-840, South Korea, namjs@gachon.ac.kr.

doi: 10.1158/1535-7163.MCT-13-0903

©2014 American Association for Cancer Research.

Downloaded from mct.aacrjournals.org on November 24, 2015. © 2014 American Association for Cancer Research.

Published OnlineFirst May 9, 2014; DOI: 10.1158/1535-7163.MCT-13-0903

kinase activity, such as SD-208 (22), SB-431542 (23), Ki26894 (24), LY-215799 (14), and LY-2109761 (25), which compete for the ATP-binding site of ALK5, have been successfully used to suppress tumor development and metastasis in animal models. In particular, LY-2157299 is currently under investigation in a clinical study of patients with metastatic malignancies to assess the ability of TGFβ inhibitors to block the expansion of chemotherapy-resistant tumor-initiating cells (14). Nonetheless, no anti-TGFβ therapy is currently available for patients with metastatic cancer. To develop anti-TGFβ therapeutics, we synthesized a novel small-molecule ALK5 inhibitor, EW-7197, and investigated its potential usefulness in anti-TGFβ therapy (26). We found that EW-7197 inhibited Smad/TGFβ signaling, cell migration, invasion, and lung metastasis in mouse mammary tumor virus (MMTV)/c-Neu and 4T1 orthotopic–grafted mice. EW-7197 also increased the survival of mice bearing 4T1 breast cancer tumors. These results demonstrate that EW-7197 represents a much more potent *in vivo* TGFβ inhibitor than those previously reported, thus providing a basis for future clinical studies.

Materials and Methods

Cell lines and culture

4T1 cells and MDA-MB-231 cells were obtained from Prof. Jeong-Seok Nam (Gachon University of Medicine and Science, Incheon, Korea) in January 2009. NMuMG cells and MCF10A cells were obtained from the ATCC in October 2008. No authentication of these cell lines was performed by the authors, with the exception of performing a mycoplasma test using the *e*-Myco plus Mycoplasma PCR Detection Kit (iNtRON BIOTECHNOLOGY) once per year. All cells were maintained in media containing penicillin (100 U/mL) and streptomycin (100 μg/mL; GenDEPOT) at 37°C in a humidified incubator in the presence of 5% CO_2. MDA-MB-231, 4T1, and NMuMG cells were grown in DMEM (GenDEPOT) containing 10% HI-FBS. Insulin (10 μg/mL; Sigma-Aldrich) was added to the NMuMG cell cultures. MCF10A cells were maintained in DMEM-F12 (1:1; Gibco) supplemented with 5% horse serum (Invitrogen), insulin (10 μg/mL), hydrocortisone (0.5 μg/mL), epidermal growth factor (20 ng/mL), and cholera toxin (100 ng/mL; Sigma-Aldrich).

Plasmids

The reporter construct, p3TP–Lux, which contains TGFβ-responsive elements, has been described previously (27). For p3TP–Lux (neo) plasmid construction, the expression cassette of the neomycin resistance gene (containing SV40 promoter and poly-A sequence) was amplified from the pGL4.17[luc2/Neo] vector (Promega) by PCR using i-MAXTM II DNA polymerase (iNtRON Biotechnology). The neomycin resistance gene was subcloned into the SalI site of the p3TP–Lux plasmid. For pGL4(CMV)–Luc (neo) plasmid construction, the expression cassette of the CMV promoter gene was amplified by PCR as described above and subcloned into the Sal I and Bgl II sites of pGL4.17[luc2/Neo]. The CMV promoter primer sequences were as follows: CMV-forward-Sac I (GAG CTC), 5′-C ACT GAG CTC TTA CGG GGT CAT TAG TTC-3′; and CMV-reverse-Bgl II (AGATCT), 5′-GCT TGA GCT CGA GAT CTG AGT CCG GTA G-3′.

Generation of 4T1 (3TP-Lux) and 4T1 (CMV-Lux) stable cells

To generate 4T1-luc [3TP-Lux (neo) and CMV-Luc (neo)] stable cells, cells were seeded at 1×10^5 cells per well in a 6-well plate. After overnight incubation, cells were transfected with the p3TP–Lux (neo) expression plasmid using the polyethyleneimine reagent (Sigma-Aldrich) according to the manufacturer's instructions, and the cells were allowed to grow in nonselective medium. Transfected cells were cultured for 4 weeks in medium containing G418 (500 μg/mL; LPS SOLUTION). Several single clones of 4T1-luc [3TP-Lux (neo)] cells were isolated and tested for luciferase expression and responsiveness to TGFβ1 treatment, and several single clones of 4T1-luc [CMV-Luc (neo)] cells were isolated and tested for luciferase activity. The clone showing the highest luciferase induction was used for the luciferase reporter gene assay [4T1-luc (3TP-Lux (neo))] and *in vivo* metastatic mouse models [4T1-luc (CMV-Luc (neo))].

Animals

BALB/c mice were purchased from Orient Bio Inc. and maintained in a temperature-controlled room (at 21°C) and supplied with food and water. MMTV/c-Neu female mice were maintained in a temperature-controlled–specific pathogen-free room (22°C) and supplied with autoclaved food and water. After the animals were sacrificed, blood and tissues were collected. Tissues were sliced into sections, snap-frozen in liquid nitrogen, and stored at −70°C. All experimental procedures were conducted in accordance with our institutional guidelines.

Breast cancer model #1 using MMTV/c-Neu mice

When the total mammary tumor volume was 100 mm^3, 32-week-old MMTV/c-Neu mice were randomized and treated (i.p.) with saline (Veh; $n = 7$) or EW-7197·HCl dissolved in saline (43.7 mg/kg; equivalent to 40 mg/kg of EW-7197, $n = 10$) three times per week for 10 weeks.

Breast cancer models #2, #3, and #4 using 4T1 orthotopic–grafted mice

In efficacy experiments (models #2 and #3), 1.2×10^4 4T1 cells were suspended in saline and implanted into the left mammary fat pads (#4) of female BALB/c mice (50 μL/mouse; day 0). Tumor size and body weight were measured weekly. Artificial gastric fluid (Veh), EW-7197 (5 or 20 mg/kg), or LY2157299 (40 or 80 mg/kg) dissolved in Veh was administered orally to mice five times per week starting from day 4 for a total of 28 days (model #2; $n = 10$/group). Veh or EW-7197 (5, 10, 20, or 40 mg/kg) was administered to mice three times per week from day 4 for a

Downloaded from mct.aacrjournals.org on November 24, 2015. © 2014 American Association for Cancer Research.

Published OnlineFirst May 9, 2014; DOI: 10.1158/1535-7163.MCT-13-0903

total of 28 days (model #3; $n = 6\sim8$/group). For the TGFβ1 challenge experiment in the model #3, 2 mice from each group were selected and treated with the indicated concentration of EW-7197 on day 28. After 30 minutes, 1 animal per group was injected (i.v.) with TGFβ1 (50 ng/mouse), and the other animal was left untreated. At 90 minutes after TGFβ1 injection, the mice were sacrificed. In survival experiments (model #4), 1.6×10^4 4T1 cells were injected as in the model #2, and Veh or EW-7197 (2.5 or 5 mg/kg) dissolved in Veh was administered orally to the mice five times per week from day 7 until death ($n = 11$/group).

The breast cancer model #5 using the 4T1-luc tail vein mouse model

4T1-luc cells [2×10^5; transfected with the plasmid construct pGL4(CMV-Luc)] were suspended in saline and injected into the tail veins of female BALB/c mice (50 μL/mouse; day 0). Artificial gastric fluid (Veh) or EW-7197 (0.625, 1.25, 2.5, or 5 mg/kg) dissolved in Veh was administered orally to mice five times per week from day 0 until death ($n = 13$/group). On day 15, surviving mice were analyzed using an *in vivo* imaging system to compare metastases in the lungs. Luciferase-positive 4T1 cells were imaged with the IVIS-200 system (Xenogen Corporation). The captured images were quantified using the Living Image Software package (PerkinElmer/Caliper Life Sciences).

Breast cancer model #6 using 4T1-luc orthotopic–grafted mice

4T1-luc cells [3×10^4; transfected with the plasmid construct pGL4(CMV-Luc)] were implanted into the left #4 mammary fat pads of female BALB/c mice as in the model #2 (day 0). Tumor size and body weight were measured weekly. Artificial gastric fluid (Veh) or EW-7197 (2.5, 5, 10, or 20 mg/kg) dissolved in Veh was administered orally to mice five times per week (2.5, 5, or 10 mg/kg) or three times per week (20 mg/kg) starting from day 4 for a total of 28 days ($n = 15$/group).

India ink staining

Mice were sacrificed, and 15% India ink solution (Hardy Diagnostics) in PBS was injected into the lung through the trachea. The number of metastatic nodules on the surface of the left lobe of the lung was counted, and images of the lungs were taken with a digital camera (Nikon).

Western blot analysis

Mouse tissues or cells were homogenized in RIPA buffer (27). Lysates containing 4 to 50 μg of total protein were separated by electrophoresis on polyacrylamide gels and then transferred electrophoretically to a polyvinylidene difluoride transfer membrane (Millipore). The membrane was blocked with 5% bovine serum albumin (Sigma-Aldrich) and incubated overnight at 4°C with the indicated primary antibodies (Supplementary Table S1). The membrane was then incubated with horseradish peroxidase–conjugated secondary antibodies. Bound antibodies were detected with the Western Blotting Luminol Reagent (Santa Cruz Biotechnology).

Wound-healing assay

4T1 cells and MDA-MB-231 cells were seeded in 6-well plates. When more than 80% of the area of each well was occupied by cells, 10% HI-FBS medium was changed to 0.2% HI-FBS medium. After 24 hours, a "wound" was made by scraping with a plastic pipette tip (time = 0), and the cells were treated with TGFβ1 (2 ng/mL) with or without ALK5 inhibitors for 24 hours (4T1) or 53 hours (MDA-MB-231). The wound area at zero time or the end point was measured using the ImageJ program according to phase-contrast images of the cells captured with a camera attached to a microscope (Carl Zeiss). The closure of the wound area was calculated as a percentage of the initial wound area.

Matrigel invasion assay

The upper surface of a Transwell (6.5-mm diameter and 8-μm pore size; Corning) was coated with 20 μL of diluted 33.3% Matrigel (BD Biosciences). 4T1 cells were seeded at 4×10^4 cells per well in the upper chamber of the Transwell in serum-free medium with or without TGFβ1 (2 ng/mL) in the presence or absence of ALK5 inhibitors. The lower chamber was filled with the same medium as in the upper chamber but with 10% HI-FBS. After incubation for 20 hours, the cells remaining on the upper surface of the membrane were removed with a cotton swab, and the DAPI-stained cells remaining on the bottom surface were observed using fluorescence microscopy (Carl Zeiss). The average cell number per field of view was obtained from five random fields.

Luciferase reporter gene assay

4T1 (3TP-Lux) stable cells (27) were seeded into a 96-well plate at 2.5×10^4 cells per well and treated with TGFβ1 (2 ng/mL) and ALK5 inhibitors in 0.2% HI-FBS medium for 24 hours. Luminescence was measured in cell lysates with a luminometer (Micro Lumat Plus; Berthold Technologies). Detailed information is described in the Supplementary Materials and Methods.

Immunofluorescence assay

Cells were fixed with 4% formaldehyde and incubated with an anti-Smad2/3 antibody (BD Biosciences) or an anti–E-cadherin antibody (Cell Signaling Technology) at 4°C overnight. Target proteins were visualized by the addition of Cy3-conjugated goat anti-mouse IgG or Alexa Fluor 488–conjugated anti-rabbit IgG (Cell Signaling Technology). Nuclei were counterstained with DAPI. Fluorescence was visualized using the LSM 510 META laser confocal microscopy system (Carl Zeiss). To visualize the infiltration of $CD8^+$ cells into the primary tumors, slides of paraffin-embedded primary tumors were incubated with PE-conjugated anti-CD8α (BD Biosciences) at 4°C overnight. Images were captured as described above.

Downloaded from mct.aacrjournals.org on November 24, 2015. © 2014 American Association for Cancer Research.

Published OnlineFirst May 9, 2014; DOI: 10.1158/1535-7163.MCT-13-0903

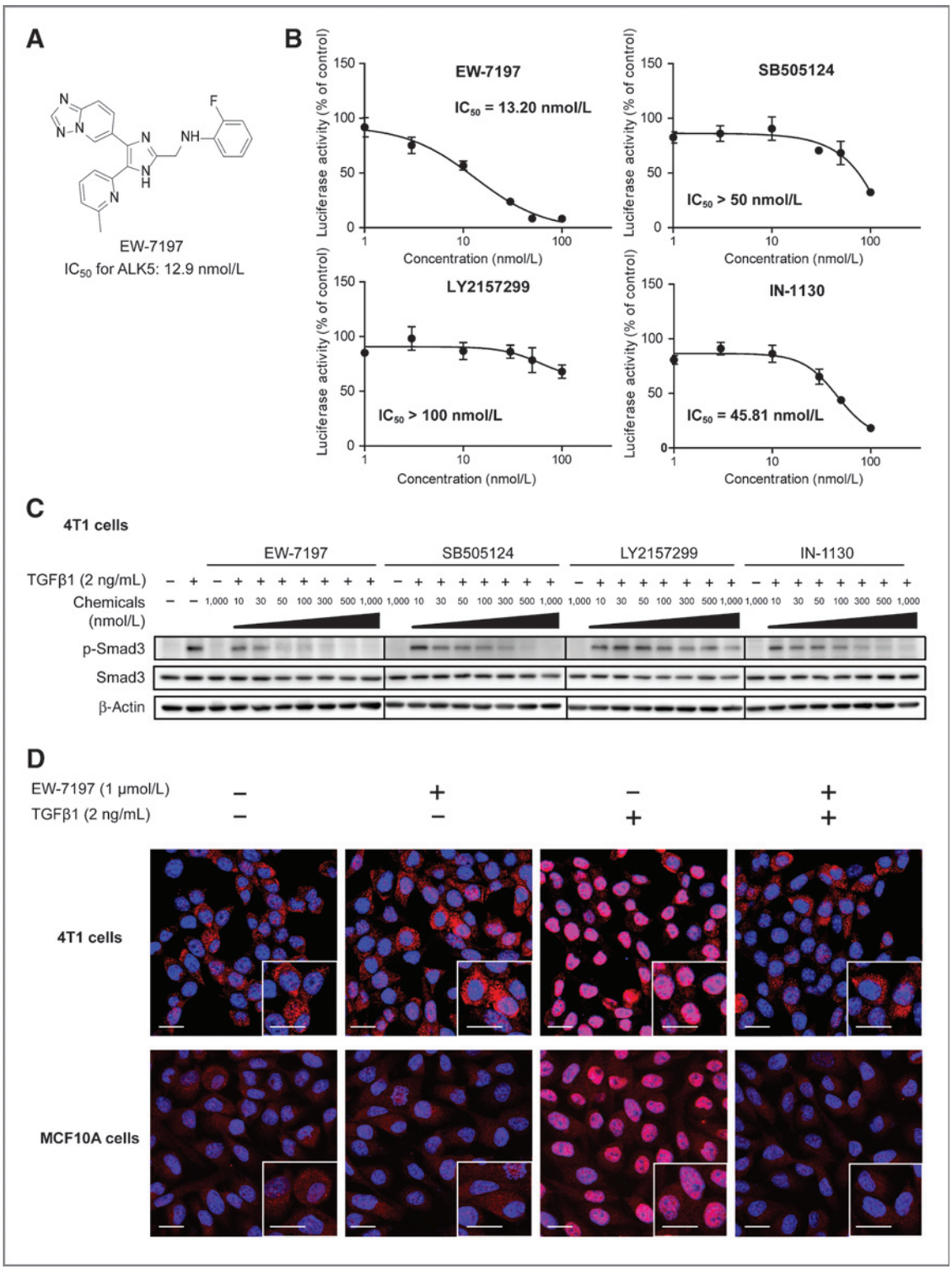

Figure 1. EW-7197 inhibits TGFβ1/Smad signaling. A, chemical structure of EW-7197. B, effects of EW-7197 on 3TP-Lux promoter activity induced by TGFβ1. The mean of luciferase activity is expressed as a percentage of the luciferase activity in the control ($n = 3$). Data, mean ± SD. The nonlinear regression (curve fit) equation was calculated using GraphPad prism. C, blockade of Smad3 phosphorylation by ALK5 inhibitors. 4T1 cells were treated with the indicated chemicals for 30 minutes with or without TGFβ1. D, blockade of Smad2/3 nuclear translocation by EW-7197. 4T1 cells and MCF10A cells were treated with EW-7197 for 2 hours with or without TGFβ1 and processed as described in Materials and Methods. Representative confocal images are presented (red, smad2/3; blue, DAPI; total magnification, ×800; scale bar, 20 μm).

Downloaded from mct.aacrjournals.org on November 24, 2015. © 2014 American Association for Cancer Research.

Published OnlineFirst May 9, 2014; DOI: 10.1158/1535-7163.MCT-13-0903

Table 1. Kinase inhibition assay against TGFβRI and p38α

	IC_{50} (nmol/L)		
Compound	**ALK5**	**P38*a***	**Selectivity index**
EW-7197	12.9	1,775	138
IN-1130	13.0	288	22
SB-505124	26.8	640	24

NOTE: IC_{50} values of the compound against TGFβRI and p38α were measured using a radiometric protein kinase assay (^{33}ProQinase Activity Assay; ProQinase), which is described in the Supplementary Materials and Methods.

RNA extraction and RT-PCR and qRT-PCR

Total RNA was isolated from mouse tissues and cells using the TRizol reagent (Invitrogen). cDNA was synthesized from 2 μg of total RNA using M-MLV reverse transcriptase (Invitrogen) and random primers (Invitrogen), and the cDNA was subjected to PCR amplification using *Taq* polymerase (Promega). Amplified DNA was analyzed by agarose gel electrophoresis. For real-time quantitative RT-PCR, cDNA was synthesized from RNA isolated from mouse tissues and cells as described above. The Power SYBR Green PCR Master Mix and Step-One Real-time PCR systems (Applied Biosystems) were used for the PCR amplification of cDNA. The primers used are listed in Supplementary Table S2.

Protein kinase assay

Selectivity profiling of EW-7197 against 320 protein kinases was performed at doses of 1×10^{-8}, 1×10^{-7}, 1×10^{-6}, and 1×10^{-5} mol/L with a radiometric protein kinase assay (^{33}ProQinase Activity Assay) provided by ProQinase (27). Detailed information is described in the Supplementary Materials and Methods.

Statistical analysis

Data are presented as the mean ± SD (*in vitro*) or mean ± SE (*in vivo*). Statistical values were defined using the Student *t* test (between two groups) or a one-way ANOVA with the Dunnett multiple comparison test (among more than two groups); *, $P < 0.05$; **, $P < 0.01$; and ***, < 0.005, respectively.

Results

EW-7197 inhibits TGFβ/Smad signaling

We synthesized EW-7197, a small-molecule ATP-competitive inhibitor of TGFβRI (ALK5), which binds to the ATP-binding site in the kinase domain of ALK5 (Fig. 1A). We compared the activity of EW-7197 with those of other ALK5 kinase inhibitors using a reporter gene assay in 4T1-3TP-Lux cells. The IC_{50} values of EW-7197, IN-1130, SB-505124, and LY-2157299 were 13.2, 45.8, >50, and >100 nmol/L, respectively, in 4T1-3TP-Lux cells (Fig. 1B). We also performed a radiometric protein kinase assay (^{33}PanQinase Activity Assay) to measure the kinase selectivity of EW-7197 over the 320 protein kinases in ProQinase (data not shown). The specificity of EW-7197 for ALK5 was 138-fold greater than that for the p38a protein kinase, which has one of the most homologous kinase domains to that of ALK5. The IC_{50} values of EW-7197 against ALK5 and p38a were 12.9 and 1775 nmol/L, respectively (Table 1). EW-7197 also inhibits ACVR1B/ALK4 and the IC_{50} value against it was determined to be 17.3 nmol/L (data not shown). EW-7197 inhibited ALK-2/ACV-R1 at concentrations comparable with ALK-5 (Supplementary Table S3). Because the ATP-binding site of the ALK5 kinase domain is essential for phosphorylation of the substrates Smad2/3, we evaluated the inhibitory effect of EW-7197 on Smad2/3 phosphorylation. EW-7197 blocked the TGFβ-induced phosphorylation of Smad2 or Smad3 in a dose-dependent manner in 4T1 cells (Fig. 1C and Supplementary Fig. S1A), NMuMG (Supplementary Fig. S1B), and MDA-MB-231 cells (Supplementary Fig. S1C). EW-7197 suppressed the TGFβ-induced nuclear translocation of Smad2/3 in 4T1 cells and MCF10A cells (Fig. 1D). The IC_{50} values of EW-7197, SB-505124, LY-2157299, and IN-1130 on pSmad3 in 4T1 cells were 10 to 30, 300 to 500, 500 to 1,000, and 300 to 500 nmol/L, respectively (Fig. 1C). EW-7197 showed a more potent inhibitory effect on TGFβ-induced Smad2 or Smad3 phosphorylation than other ALK5 inhibitors previously identified.

EW-7197 abrogates TGFβ1-induced tumor cell migration and invasion

TGFβ1 is known to stimulate the migration of tumor cells (28). To study the effect of EW-7197 on the cellular migration and invasion mediated by TGFβ1, we performed wound-healing and Matrigel invasion assays. In the wound-healing assay, we compared the effect of EW-7197 with that of other ALK5 inhibitors, such as SB-505124, IN-1130, and LY-2157299, at various concentrations (0.1, 0.5, and 1 μmol/L) in 4T1 cells and MDA-MB-231 cells. TGFβ1 accelerated cell motility and wound closure, and EW-7197 showed stronger inhibition of TGFβ1-induced cell migration than SB-5050124 or LY-2157299 (Fig. 2A and B and Supplementary Fig. S2A). In the Matrigel invasion assay, TGFβ1 enhanced the invasion of 4T1 cells by 3-fold and EW-7197 strongly attenuated TGFβ1-induced cell invasion. However, LY-2157299 did not inhibit cell invasion at a concentration of 1 μmol/L (Fig. 2C). We also examined whether the inhibitory effect

Downloaded from mct.aacrjournals.org on November 24, 2015. © 2014 American Association for Cancer Research.

Published OnlineFirst May 9, 2014; DOI: 10.1158/1535-7163.MCT-13-0903

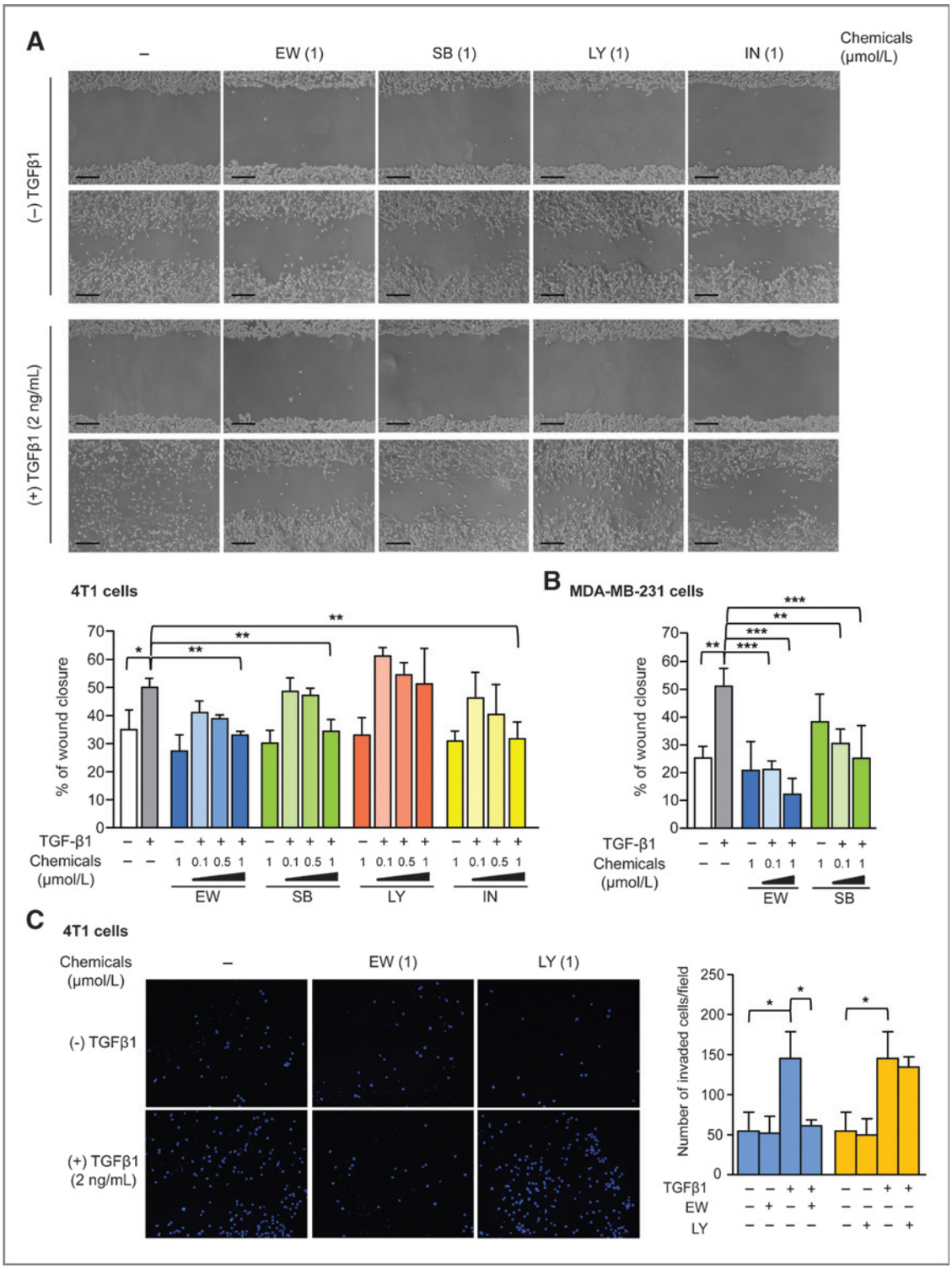

Figure 2. Effect of EW-7197 on cell migration and invasion. Wound-healing assays (described in Materials and Methods) using 4T1 cell for 24 hours (A) and MDA-MB-231 cell for 53 hours (B). Representative phase-contrast images are presented (total magnification, ×100; scale bar, 100 μm). Data, mean ± SD of the closed wound area shown as a percentage of the initial wound area ($n = 4$). Statistical significance was defined using one-way ANOVA with the Dunnett multiple comparison test. C, Matrigel invasion assay using 4T1 cells (described in Materials and Methods). Representative fluorescence images are presented (total magnification, ×100; scale bar, 100 μm). Data, mean ± SD of the number of invaded cells per field of view ($n = 3$). Statistical significance was defined as described above; *, $P < 0.05$; **, $P < 0.01$, and ***, $P < 0.005$, respectively.

Downloaded from mct.aacrjournals.org on November 24, 2015. © 2014 American Association for Cancer Research.

Published OnlineFirst May 9, 2014; DOI: 10.1158/1535-7163.MCT-13-0903

of EW-7197 on cell migration and invasion was due to the inhibition of cell proliferation, and we found that EW-7197 did not affect the proliferation of 4T1 and MCF10A cells (Supplementary Fig. S2B and S2C), although EW-7197 inhibited 4T1 cell proliferation when added at a high concentration (5,000 nmol/L). Thus, EW-7197 strongly suppressed the TGFβ1-induced migration and invasion of breast cancer cells.

EW-7197 inhibits EMT in breast cancer cells

TGFβ induces the progression of epithelial cancer and promotes metastasis via the alteration of cellular plasticity, loss of cell–cell contact, increased cell migration, increased invasion, and degradation of the extracellular matrix. The EMT in epithelial cells is characterized by the acquisition of a spindle morphology and increased motility with the loss of the tight and adherent junctions (12, 29, 30). To examine the effect of EW-7197 on TGFβ1-induced EMT, we used mouse mammary epithelial cells (NMuMG) and immortalized human mammary epithelial cells (MCF10A). TGFβ1 treatment changed the morphology of NMuMG cells from a cuboidal shape to an elongated spindle-like shape and from a dense distribution to a sparse distribution within 48 hours (Fig. 3A), which was consistent with previous studies (12). EW-7197 also inhibited the change in morphology induced by TGFβ1 more efficiently than SB-505124 and LY-2157299. E-Cadherin is known to be one of the cell–cell interaction proteins that is destroyed during TGFβ1-induced EMT. We confirmed E-cadherin protein expression using an immunofluorescence assay with confocal microscopy. EW-7197 inhibited the TGFβ1-induced delocalization and the loss of E-cadherin expression in NMuMG cells (Fig. 3B). We further confirmed by Western blot analysis that TGFβ1 reduced the expression of E-cadherin, but increased that of N-cadherin, Snail, and Fibronectin, and these changes were reversed by concomitant treatment with EW-7197 and TGFβ1 in MCF10A cells (Fig. 3C). For a more detailed comparison, we performed experiments using a broad range of concentrations of other ALK5 inhibitors. EW-7197 inhibited the morphologic change induced by TGFβ1 at a lower concentration than other ALK5 inhibitors (Supplementary Fig. S3A). At the same time, EW-7197 restored E-cadherin expression, which was reduced by TGFβ1, whereas it ameliorated N-cadherin expression, which was induced by TGFβ1, at a lower concentration than other ALK5 inhibitors (Supplementary Fig. S4A). As TGFβ induces EMT through transcriptional regulation, we examined the effect of EW-7197 on transcriptional regulators, such as *SNAI1*, *SNAI2*, and *HMGA2*, as well as markers of EMT, such as *CDH1* and *FN*. TGFβ1 downregulated the mRNA level of *CDH1* and upregulated the mRNA levels of *FN1*, *HMGA2* (high-mobility group AT-hook 2), *SNAI1*, and *SNAI2* (Snail family zinc finger 1 and 2, respectively). Moreover, EW-7197 abolished the TGFβ1-induced effects on genes related to EMT (Fig. 3D). The inhibition of TGFβ1-induced EMT by EW-7197 may be mediated through the regulation of mRNA and protein levels, and EW-7197 showed potent inhibition of EMT compared with SB-505124.

EW-7197 inhibits breast cancer metastasis to the lung

Epidemiologic analysis of a cohort of 615 human breast tumors has shown that the TGFβ signaling pathway may be linked to breast cancer metastasis to the lung (28). EW-7197 (40 mg/kg) treatment of MMTV/c-Neu transgenic mice significantly reduced lung metastasis by 60% compared with the control, based on *Csn2* (β-*casein*) mRNA levels in the lung tissue (Fig. 4A). We confirmed the tumor burden in metastasized lungs by hematoxylin and eosin (H&E) staining (Supplementary Fig. S5A). The total tumor volume and body weight did not differ between saline- (Veh) and EW-7197–treated groups (Supplementary Fig. S5B and S5C). To examine the antimetastatic effect of EW-7197 on breast cancer metastasis to the lung *in vivo*, the BALB/c 4T1 metastatic breast cancer model was established. Specifically, 4T1 cells were transplanted into the mammary fat pads of BALB/c mice (day 0), which were treated with either artificial gastric fluid (Veh), EW-7197 (5 or 20 mg/kg) or LY2157299 (40 or 80 mg/kg) orally five times per week from day 4 to day 28. Treatment with EW-7197 and LY2157299 decreased the number of metastatic nodules compared with that in the Veh-treated control group by 53% and 68% (5 and 20 mg/kg) and by 33% and 53% (40 and 80 mg/kg), respectively (Fig. 4B). EW-7197 showed a more potent inhibitory effect on the metastasis of breast cancer cells to the lung than LY2157299. There was no difference in primary tumor size (Fig. 4C) or body weight (Supplementary Fig. S5D) between the Veh-treated group and the EW-7197– or LY2157299-treated group. Because treatment with 5 mg/kg EW-7197 every day for 5 days per week showed the maximal effect, we performed EW-7197 treatment (5, 10, 20, or 40 mg/kg) every other day (three times/week) from day 4 to day 28 to examine a possible dose relationship. The results showed that EW-7197 decreased the number of metastatic nodules in a dose-dependent manner without inducing any effects on the primary tumor size or body weight (Fig. 4D and E and Supplementary Fig. S5E), and the efficacy of EW-7197 reached a plateau after 20 mg/kg. In TGFβ1 challenge experiments, EW-7197 inhibited Smad2 phosphorylation in primary tumors in a dose-dependent manner (Supplementary Fig. S5F).

EW-7197 prolongs the life span of BALB/c 4T1 mice via inhibition of EMT

EW-7197 (5 mg/kg five times/week) treatment was sufficient to produce the maximal antimetastatic effect. EW-7197 (0.625, 1.25, 2.5, or 5 mg/kg; five times/week) inhibited lung metastasis and increased the survival of 4T1-Luc cells, which were injected via the tail vein into BALB/c mice, in a dose-dependent manner (Fig. 5A and B). On the 22nd day, the percentage of surviving control mice was 7.7%, whereas the percentage of surviving mice

Downloaded from mct.aacrjournals.org on November 24, 2015. © 2014 American Association for Cancer Research.

Published OnlineFirst May 9, 2014; DOI: 10.1158/1535-7163.MCT-13-0903

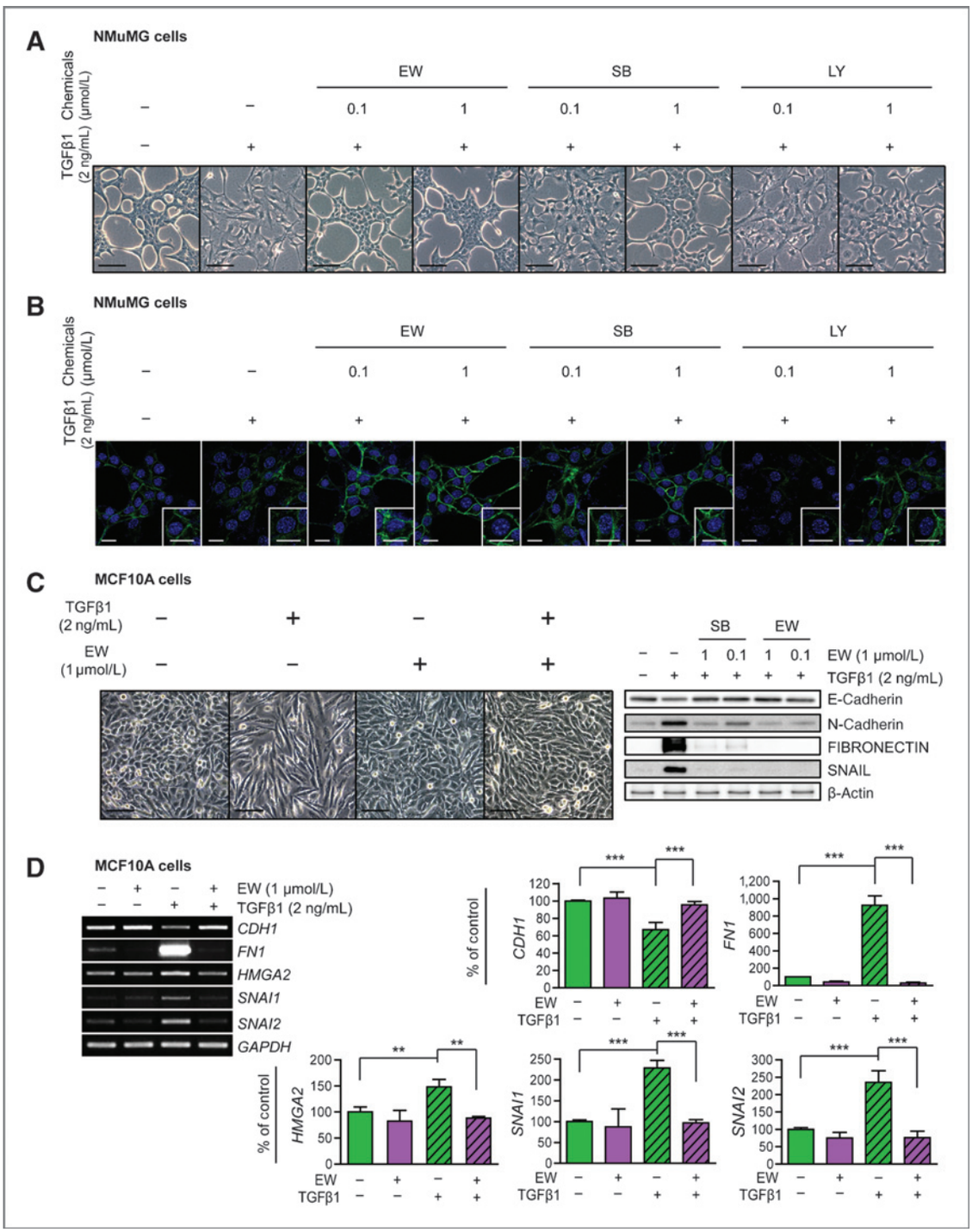

Figure 3. Effect of EW-7197 on EMT. A and B, NMuMG cells were treated with TGFβ1 (2 ng/mL) with or without ALK5 inhibitors in serum-reduced (5% HI-FBS) medium for 2 days. A, cell morphology was observed by phase-contrast microscopy (total magnification, ×100; scale bar, 100 μm). B, for visualization of E-cadherin (green), NMuMG cells were cultured as described above and processed as described in Materials and Methods. Representative confocal images are presented (blue, DAPI; total magnification, ×400; scale bar, 20 μm). C and D, MCF10A cells were treated with TGFβ1 (2 ng/mL) in 0.2%% HI-FBS medium with or without ALK5 inhibitors. C, after 96 hours, cell morphology was observed by phase-contrast microscopy (total magnification, ×100; scale bar, 100 μm) and total protein was isolated and analyzed using specific antibodies against EMT markers (E-cadherin, N-cadherin, SNAIL, and fibronectin) by Western blotting. β-Actin was used for endogenous reference. D, total RNA was isolated and mRNA transcript levels of *CDH1*, *FN1*, *HMGA2*, *SNAI1*, and *SNAI2* were analyzed by RT-PCR. Data were normalized against *GAPDH*. Data, mean ± SD ($n = 3$). Statistical significance was defined by one-way ANOVA with the Dunnett multiple comparison test; **, $P < 0.01$ and ***, $P < 0.005$, respectively.

Downloaded from mct.aacrjournals.org on November 24, 2015. © 2014 American Association for Cancer Research.

Published OnlineFirst May 9, 2014; DOI: 10.1158/1535-7163.MCT-13-0903

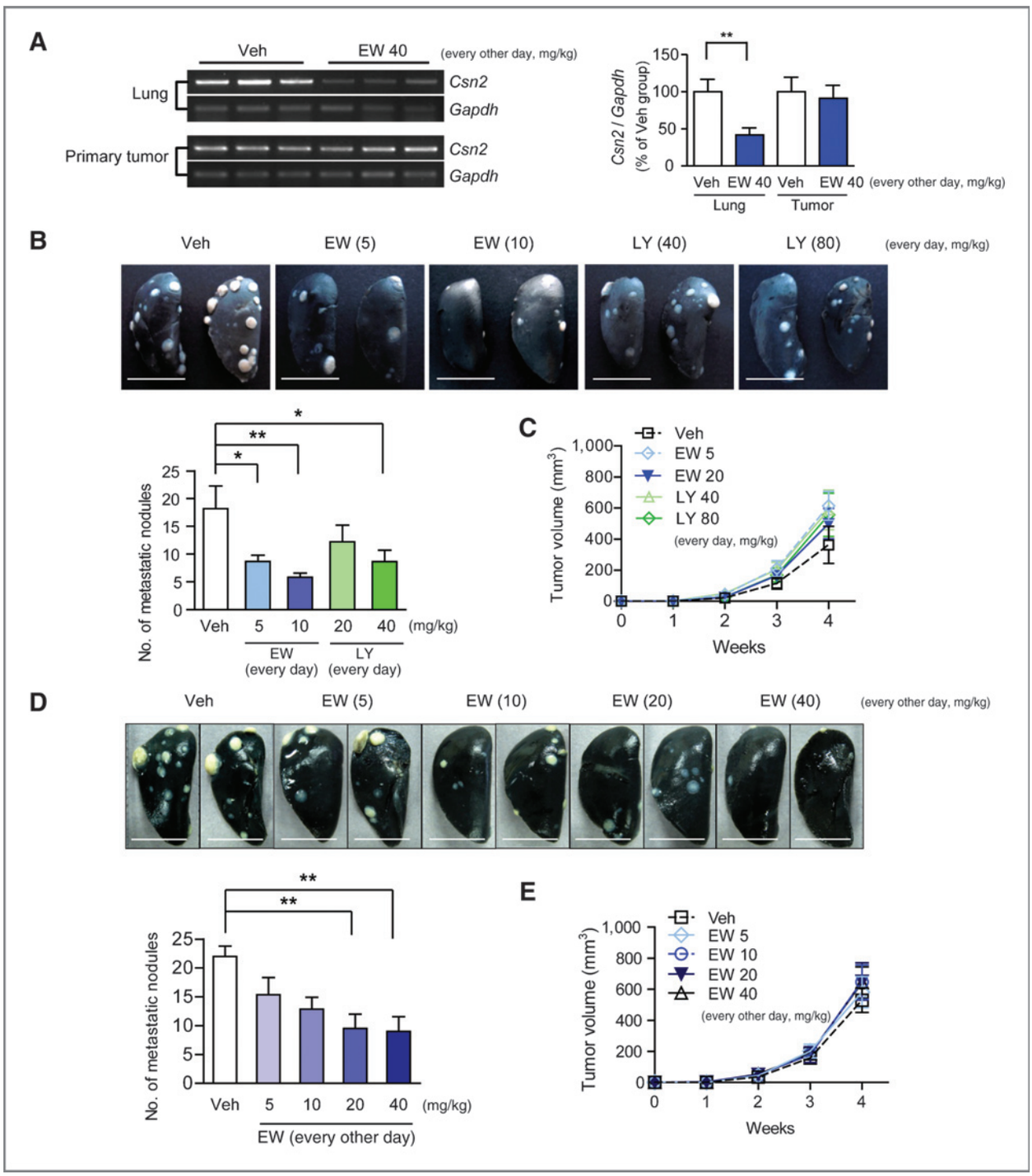

Figure 4. EW-7197 inhibits breast cancer metastasis to the lung. A, EW-7197 inhibited lung metastasis of the breast tumor *in vivo* breast cancer model #1 (described in Materials and Methods). Inhibition of lung metastasis by EW-7197 (40 mg/kg) in MMTV/c-Neu mice was evaluated by measuring the mRNA expression of *Csn2* (β-*casein*) in lungs using RT-PCR. Data were normalized against *Gapdh*. Data, mean ± SE (Veh, $n = 7$; EW, $n = 10$). Statistical significance was defined using the Student *t* test. B and C, the breast cancer model #2 (described in Materials and Methods). B, inhibition of lung metastasis by EW-7197 was evaluated by India ink staining. Representative images of lungs with metastatic nodules (white spots) are shown (top; scale bar, 1 cm). Data, number of metastatic nodules as the mean ± SE ($n = 10$/group; bottom). Statistical significance was defined using one-way ANOVA with the Dunnett multiple comparison test. C, effects of EW-7197 on primary tumor volume. D and E, the breast cancer model #3 (described in Materials and Methods). D, inhibition of lung metastasis by EW-7197 was evaluated by India ink staining. Representative images of lungs (top) and the number of metastatic nodules (bottom) are presented as described above ($n = 6\sim8$/group). Statistical values were defined as above. E, effects of EW-7197 on primary tumor volume; *, $P < 0.05$ and **, $P < 0.01$, respectively.

Downloaded from mct.aacrjournals.org on November 24, 2015. © 2014 American Association for Cancer Research.

Published OnlineFirst May 9, 2014; DOI: 10.1158/1535-7163.MCT-13-0903

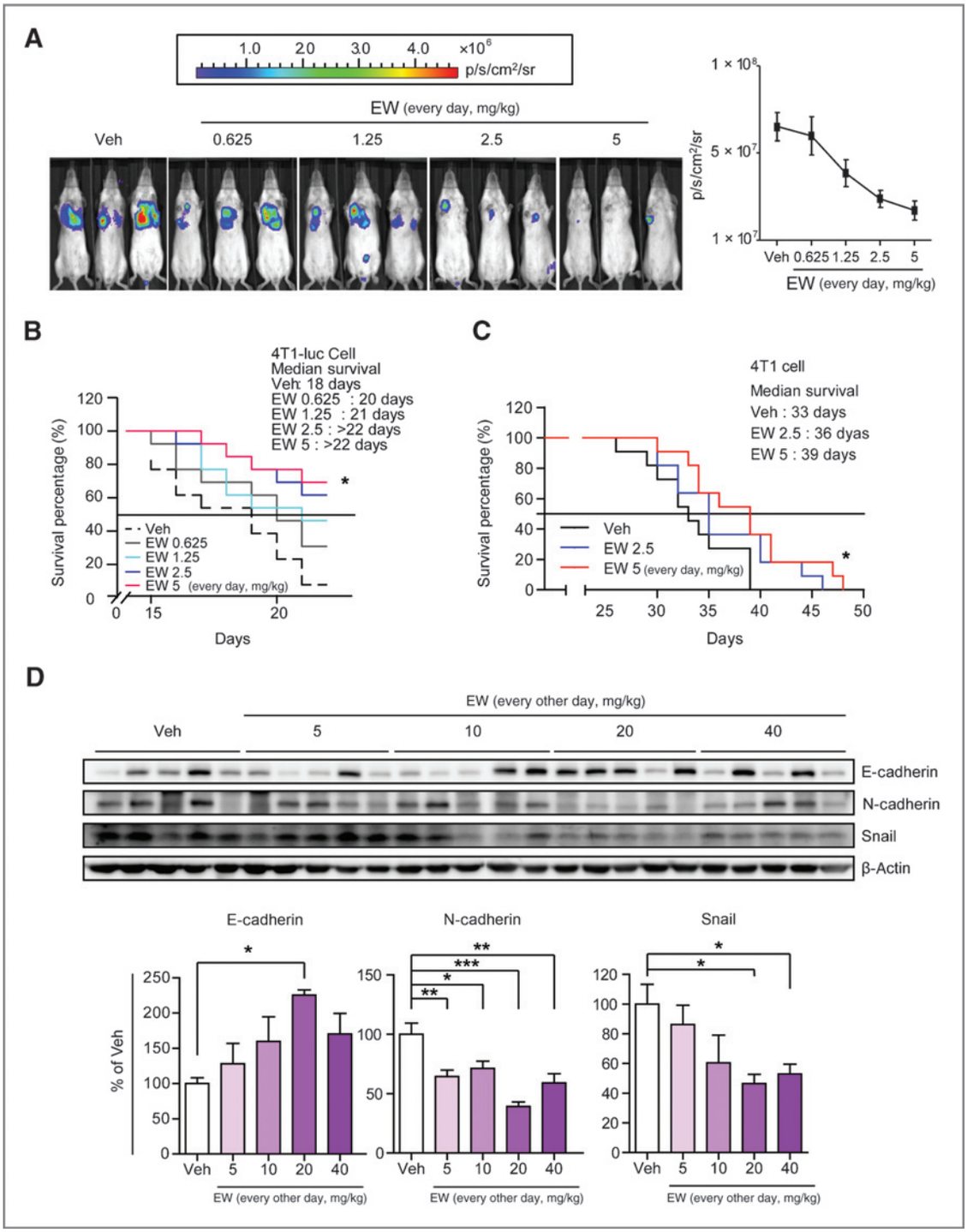

Figure 5. EW-7197 prolongs the life span of BALB/c 4T1 mice via inhibition of EMT. A and B, the breast cancer model #5 (described in Materials and Methods). A, metastasis to the lungs was visualized by bioluminescence analysis as described in Materials and Methods. The image (left) shows the region of metastatic area in three representative mice per each group. Data, mean ± SE ($n = \sim$13/group). B, effect of EW-7197 on survival. Data, the percentage of survival in each group on the indicated day ($n = 13$/group). Kaplan–Meier curves were produced using GraphPad Prism. Statistical values were defined using the log-rank test. C, the breast cancer model #4 (described in Materials and Methods). Effect of EW-7197 on survival ($n = 11$/group). Survival curves and statistical values were produced as described above. D, the breast cancer model #3 (described in Materials and Methods). Effect of EW-7197 on EMT in primary tumors. Western blots (top) and quantification of all samples from each group (bottom). Data were normalized to β-actin. Data, mean ± SE ($n = 5$/group) shown as a percentage of the artificial gastric fluid (Veh)–treated group. Statistical significance was defined using one-way ANOVA with the Dunnett multiple comparison test; *, $P < 0.05$; **, $P < 0.01$, and ***, $P < 0.005$, respectively.

Downloaded from mct.aacrjournals.org on November 24, 2015. © 2014 American Association for Cancer Research.

Published OnlineFirst May 9, 2014; DOI: 10.1158/1535-7163.MCT-13-0903

treated with EW-7917 at 0.625, 1.25, 2.5, and 5 mg/kg was 30.8, 46.1, 61.5, and 69.2%, respectively (Fig. 5B). EW-7197 also prolonged the survival of BALB/c mice orthotopically bearing 4T1 tumors by 36% at doses of 2.5 and 5 mg/kg (Fig. 5C). These findings suggested that EW-7197 inhibited the lung metastasis of breast tumor cells, thereby enhancing the life-span of mice bearing breast tumors. To further investigate the mechanism of the effect of EW-7197 on metastasis, we analyzed the protein levels of EMT markers in primary tumors by Western blotting. EW-7197 treatment increased E-cadherin and decreased Snail expression in a dose-dependent manner (Fig. 5D), and N-cadherin was also decreased by EW-7197 treatment (Fig. 5D). These results indicated that EW-7197 may inhibit metastasis to the lung *in vivo* via the inhibition of EMT, although this compound did not affect primary tumor growth.

EW-7197 inhibits metastasis and enhances the activity of cytotoxic T lymphocytes in 4T1 orthotopic–grafted mice

EMT profoundly alters the susceptibility of cancer cells to T-cell–mediated immune surveillance (30). Therefore, we next tested whether EW-7197 treatment would affect immune surveillance. We performed an immunofluorescence assay in primary tumors of 4T1 orthotopic–grafted mice against the CD8 protein, which is expressed on the surface of cytotoxic T lymphocytes (CTL). The intensity of the $CD8^+$ area showed that EW-7197 increased the infiltration of $CD8^+$ immune cells into primary tumors (Fig. 6A and B). We confirmed these results by measuring the mRNA level of CD8 (*Cd8b1*) in primary tumors relative to that of peptidylprolyl isomerase A (cyclophilin A, *Ppia*), an endogenous housekeeping gene, using real-time qPCR (Fig. 6B). Because the cytolytic activity and number of

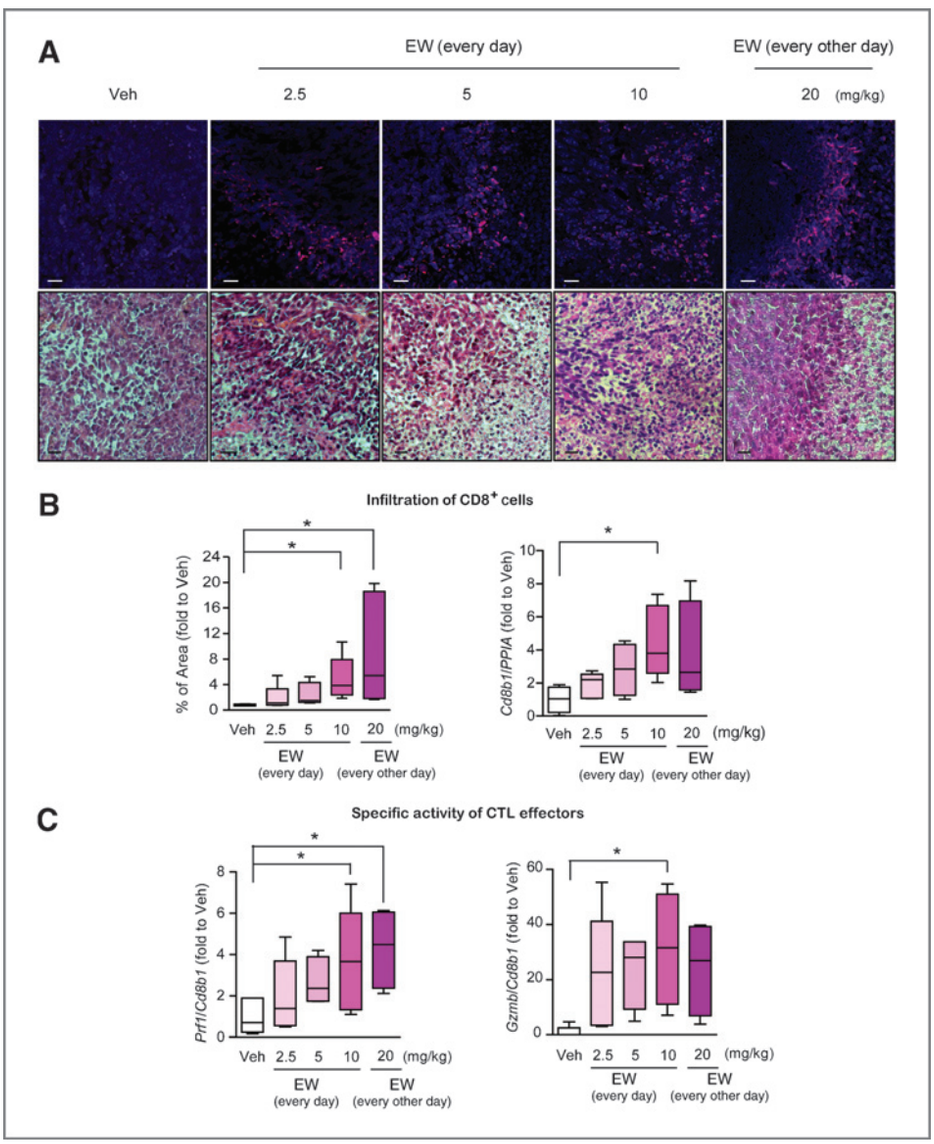

Figure 6. EW-7197 inhibits metastasis and enhances the activity of CTLs in 4T1 orthotopic–grafted mice. A to C, the breast cancer model #6 (described in Materials and Methods). Effect of EW-7197 on the infiltration of $CD8^+$ cells in primary breast tumors. A, the $CD8^+$ cells in primary tumors were visualized by immunofluorescence staining (described in Materials and Methods). Representative confocal images are presented (total magnification, ×400; scale bar, 25 μm; red, Cd8α; blue, DAPI) and matched with H&E-stained images. B, $Cd8\alpha^+$ area (above) was calculated as the percentage of the total field and presented as fold to the artificial gastric fluid (Veh)–treated group. The mRNA level of *Cd8b1* in primary breast tumors was analyzed by qRT-PCR and normalized by *Ppia* ($n = 4\sim7$/group). Statistical significance was defined using one-way ANOVA with the Dunnett multiple comparison test. C, effect of EW-7197 on the activity of CTLs. Cytolytic activity of CTLs was measured by qRT-PCR analysis of *Prf1* and *Gzmb* expression normalized to *Cd8b1* in primary breast tumors. Boxes, median values with the upper and lower quartiles, and whiskers, the range ($n = 4\sim7$/group). Statistical significance was defined as described above. *, $P < 0.05$.

Downloaded from mct.aacrjournals.org on November 24, 2015. © 2014 American Association for Cancer Research.

Published OnlineFirst May 9, 2014; DOI: 10.1158/1535-7163.MCT-13-0903

CTLs are important, we analyzed the cytolytic effector functions of CTLs, such as perforin, which forms pores on the membrane of target cells, and granzyme B, a catalytic enzyme released from CTLs into the cytosol of target cells. The cytolytic activity of CTLs was analyzed by measuring the expression of perforin (*Prf1*) and granzyme B (*Gzmb*) relative to that of CD8. The results showed that the cytolytic activity of CTLs was increased following EW-7197 treatment in a dose-dependent manner (Fig. 6C). At the same time, EW-7197 decreased lung metastasis in a dose-dependent manner without any effects on primary tumor size (Supplementary Fig. S6). This finding may suggest that EW-7197 inhibits the pulmonary metastasis of breast cancer and improves immune surveillance in terms of CTL activity and recruitment.

Discussion

TGFβ inhibitors are being developed as antimetastatic agents for treating patients with cancer because TGFβ has a variety of antitumorigenic effects (16–25, 31). Although ligand traps, such as 1D11 (17), and antisense-specific oligos (ASO), such as AP12009 (32), limit the bioavailability of active TGFβ ligands, they fail to directly block signaling through the receptor. Moreover, small-molecule inhibitors of TGFβ receptor kinases can block receptor signaling, although such kinase inhibitors demonstrate lower specificity than ASOs or mAbs. Previous studies suggest that many small-molecule inhibitors of TGFβRI/ALK5 also inhibit the related activin and nodal receptors, namely ACVR1B/ALK4 and ACVR1C/ALK7, but with a reduced affinity (32, 33). EW-7197 also inhibited TGFβRI/ALK5 (IC_{50} = 12.9 nmol/L) and ACVR1B/ALK4 (IC_{50} = 17.3 nmol/L), but the specificity of EW-7197 for ALK5 inhibition was 138-fold greater than that for the p38a protein kinase (Table 1). Although EW-7197 is designed to have a great specificity to ALK-5, we cannot rule out the possibility that the inhibition of ALK-2/ACV-R1 may also contribute to some of the phenotypic responses and *in vivo* activity observed in the present studies. It has been more difficult to demonstrate a significant reduction in primary tumors, although TGFβ signaling inhibition results in a significant reduction in metastasis in mouse models. Similarly, EW-7197 was found to inhibit the lung metastasis of breast tumors in mouse models without affecting the primary tumor size (Fig. 4). These facts suggest that combinatorial therapy may enhance the efficacy of TGFβ inhibitors in clinical practice. The TGFβRI/II kinase inhibitor, LY-2109761, in combination with temozolomide and radiotherapy in a glioblastoma model was shown to inhibit tumor growth compared with controls (25). Furthermore, loss of TGFβ signaling can increase the therapeutic efficacy of cancer treatment with rapamycin (34) and doxorubicin (35). In the 4T1 mouse model, a combination of ixabepilone, capecitabine, and 1D11 treatment reduces primary tumor growth and metastasis (36), and this combinatorial treatment has also shown some efficacy for patients with breast cancer resistant to anthracycline and taxane therapy (36). Metastatic triple-negative breast cancers often recur after chemotherapy (37), and metastatic tumor relapses are characterized by rapid cellular proliferation due to the survival of a small population of cells with stem-like properties and drug resistance (8–10). Thus, it would be interesting to examine whether EW-7197 may improve the efficacy of paclitaxel in combinatorial treatment. The reference suggested that cells that harbor autocrine TGFβ signaling are causally associated with resistance to paclitaxel (14) and TGFβ-induced EMT has been associated with the acquisition of tumor stem-like properties (13). The TGFβ signaling pathway is involved in the maintenance of cancer stem cells in breast carcinomas (14). Indeed, a TGFβRI/II kinase inhibitor was shown to reverse EMT and induce mesenchymal-to-epithelial differentiation in $CD44^+$ mammary epithelial cells (15). This study demonstrated that the novel small-molecule TGFβ receptor I kinase ALK5 inhibitor, EW-7197, inhibited Smad/TGFβ signaling, EMT, cell migration, invasion, and lung metastasis in orthotopic-grafted mice. Furthermore, EW-7197 increased the survival time of mice bearing 4T1-Luc breast tumors.

In summary, EW-7197 could be used as an antimetastatic drug in oncology. Our data strongly indicate that our novel small-molecule ALK5 inhibitor, EW-7197, showed therapeutic antimetastatic effects in 4T1 breast tumor-bearing mice. However, further clinical studies and trials are necessary to validate the therapeutic potential of EW-7197.

Disclosure of Potential Conflicts of Interest

No potential conflicts of interest were disclosed.

Authors' Contributions

Conception and design: Y.Y. Sheen
Development of methodology: Y.Y. Sheen
Acquisition of data (provided animals, acquired and managed patients, provided facilities, etc.): S.W. Kim, D.-K. Kim, Y.Y. Sheen
Analysis and interpretation of data (e.g., statistical analysis, biostatistics, computational analysis): J.Y. Son, S.-Y. Park, S.-J Kim, S.J. Lee, S.-A. Park, M.-J. Kim, J.-S. Nam, Y.Y. Sheen
Writing, review, and/or revision of the manuscript: S.-Y. Park, J.-S. Nam, Y.Y. Sheen
Administrative, technical, or material support (i.e., reporting or organizing data, constructing databases): S.W. Kim, Y.Y. Sheen
Study supervision: Y.Y. Sheen
Other (preparing the target molecule, EW-7197): D.-K. Kim

Acknowledgments

The authors thank the following individuals: Dr. Sri Ram (NIH/Retired) and Dr. Lalage M. Wakefield (NIH) for critical review and discussion of article; Min-Kyung Park and Jung In Jee for maintaining animals and collecting tissue samples; and Jung-shin Kim for excellent technical support.

Grant Support

This work was supported by Korea Science and Engineering Foundation (KOSEF) grant funded by the Korea government (MEST; no. 20090093972; to all authors).

The costs of publication of this article were defrayed in part by the payment of page charges. This article must therefore be hereby marked *advertisement* in accordance with 18 U.S.C. Section 1734 solely to indicate this fact.

Received October 21, 2013; revised April 30, 2014; accepted April 30, 2014; published OnlineFirst May 9, 2014.

Downloaded from mct.aacrjournals.org on November 24, 2015. © 2014 American Association for Cancer Research.

Published OnlineFirst May 9, 2014; DOI: 10.1158/1535-7163.MCT-13-0903

References

1. Taylor MA, Parvani JG, Schiemann WP. The pathophysiology of epithelial–mesenchymal transition induced by transforming growth factor-β in normal and malignant mammary epithelial cells. J Mammary Gland Biol Neoplasia 2010;15:169–90.
2. Massagué J. How cells read TGF-β signals. Nat Rev Mol Cell Biol 2000;1:169–78.
3. Brown KA, Pietenpol JA, Moses HL. A tale of two proteins: differential roles and regulation of Smad2 and Smad3 in TGF-β signaling. J Cell Biochem 2007;101:9–33.
4. Bierie B, Moses HL. Tumour microenvironment: TGFβ: the molecular Jekyll and Hyde of cancer. Nat Rev Cancer 2006;6:506–20.
5. Shi Y, Massagué J. Mechanisms of TGF-β signaling from cell membrane to the nucleus. Cell 2003;113:685–700.
6. Connolly EC, Akhurst RJ. The complexities of TGF-β action during mammary and squamous cell carcinogenesis. Curr Pharm Biotechnol 2011;12:2138.
7. Shipitsin M, Campbell LL, Argani P, Weremowicz S, Bloushtain-Qimron N, Yao J, et al. Molecular definition of breast tumor heterogeneity. Cancer Cell 2007;11:259–73.
8. Al-Hajj M, Wicha MS, Benito-Hernandez A, Morrison SJ, Clarke MF. Prospective identification of tumorigenic breast cancer cells. Proc Natl Acad Sci U S A 2003;100:3983–8.
9. Dalerba P, Cho RW, Clarke MF. Cancer stem cells: models and concepts. Annu Rev Med 2007;58:267–84.
10. McDermott SP, Wicha MS. Targeting breast cancer stem cells. Mol Oncol 2010;4:404–19.
11. Li X, Lewis MT, Huang J, Gutierrez C, Osborne CK, Wu MF, et al. Intrinsic resistance of tumorigenic breast cancer cells to chemotherapy. J Natl Cancer Inst 2008;100:672–9.
12. Lindley LE, Briegel KJ. Molecular characterization of TGFβ-induced epithelial–mesenchymal transition in normal finite lifespan human mammary epithelial cells. Biochem Biophys Res Commun 2010;399:659–64.
13. Mani SA, Guo W, Liao M-J, Eaton EN, Ayyanan A, Zhou AY, et al. The epithelial–mesenchymal transition generates cells with properties of stem cells. Cell 2008;133:704–15.
14. Bhola NE, Balko JM, Dugger TC, Kuba MG, Sánchez V, Sanders M , et al. TGF-β inhibition enhances chemotherapy action against triple-negative breast cancer. J Clin Invest 2013;123:1348.
15. Saunier EF, Akhurst RJ. TGF beta inhibition for cancer therapy. Curr Cancer Drug Targets 2006;6:565–78.
16. Schlingensiepen KH, Fischer-Blass B, Schmaus S, Ludwig S. Antisense therapeutics for tumor treatment: the TGF-beta2 inhibitor AP 12009 in clinical development against malignant tumors. Recent Results Cancer Res 2008:177;137–50.
17. Nam J-S, Terabe M, Mamura M, Kang M-J, Chae H, Stuelten C, et al. An anti-transforming growth factor β antibody suppresses metastasis via cooperative effects on multiple cell compartments. Cancer Res 2008;68:3835–43.
18. Yang Ya, Dukhanina O, Tang B, Mamura M, Letterio JJ, MacGregor J, et al. Lifetime exposure to a soluble TGF-β antagonist protects mice against metastasis without adverse side effects. J Clin Invest 2002;109:1607–15.
19. Seth P, Wang ZG, Pister A, Zafar MB, Kim S, Guise T, et al. Development of oncolytic adenovirus armed with a fusion of soluble transforming growth factor-β receptor II and human immunoglobulin Fc for breast cancer therapy. Hum Gene Ther 2006;17:1152–61.
20. Hu Z, Zhang Z, Guise T, Seth P. Systemic delivery of an oncolytic adenovirus expressing soluble transforming growth factor-β receptor II–Fc fusion protein can inhibit breast cancer bone metastasis in a mouse model. Hum Gene Ther 2010;21:1623–9.
21. Bandyopadhyay A, López-Casillas F, Malik SN, Montiel JL, Mendoza V, Yang J, et al. Antitumor activity of a recombinant soluble betaglycan in human breast cancer xenograft. Cancer Res 2002;62:4690–5.
22. Mohammad KS, Javelaud D, Fournier PG, Niewolna M, McKenna CR, Peng XH , et al. TGF-β-RI kinase inhibitor SD-208 reduces the development and progression of melanoma bone metastases. Cancer Res 2011;71:175–84.
23. Tanaka H, Shinto O, Yashiro M, Yamazoe S, Iwauchi T, Muguruma K, et al. Transforming growth factor β signaling inhibitor, SB-431542, induces maturation of dendritic cells, and enhances anti-tumor activity. Oncol Rep 2010;24:1637–43.
24. Ehata S, Hanyu A, Fujime M, Katsuno Y, Fukunaga E, Goto K, et al. Ki26894, a novel transforming growth factor-β type I receptor kinase inhibitor, inhibits *in vitro* invasion and *in vivo* bone metastasis of a human breast cancer cell line. Cancer Sci 2007;98:127–33.
25. Zhang M, Kleber S, Röhrich M, Timke C, Han N, Tuettenberg J, et al. Blockade of TGF-β signaling by the TGFβR-I kinase inhibitor LY2109761 enhances radiation response and prolongs survival in glioblastoma. Cancer Res 2011;71:7155–67.
26. Kim DK, Sheen YY, Chenghua J, Park CY, Sreenu D, Sudhakar RK; inventors. 2-Pyridyl substituted imidazoles as therapeutic ALK5 and/or ALK4 inhibitors. United States patent US 8080568B1. 2011 Dec 20.
27. Park CY, Son JY, Jin CH, Nam JS, Kim DK, Sheen YY. EW-7195, a novel inhibitor of ALK5 kinase inhibits EMT and breast cancer metastasis to lung. Eur J Cancer 2011;47:2642–53.
28. Zhang XHF, Wang Q, Gerald W, Hudis CA, Norton L, Smid M, et al. Latent bone metastasis in breast cancer tied to Src-dependent survival signals. Cancer Cell 2009;16:67–78.
29. Giampieri S, Pinner S, Sahai E. Intravital imaging illuminates transforming growth factor β signaling switches during metastasis. Cancer Res 2010;70:3435–9.
30. Akalay I, Janji B, Hasmim M, Noman MZ, André F, De Cremoux P, et al. Epithelial-to-mesenchymal transition and autophagy induction in breast carcinoma promote escape from T-cell–mediated lysis. Cancer Res 2013;73:2418–27.
31. Bandyopadhyay A, Agyin JK, Wang L, Tang Y, Lei X, Story BM, et al. Inhibition of pulmonary and skeletal metastasis by a transforming growth factor-β type I receptor kinase inhibitor. Cancer Res 2006;66:6714–21.
32. Hau P, Jachimczak P, Schlingensiepen R, Schulmeyer F, Jauch T, Steinbrecher A, et al. Inhibition of TGF-β 2 with ap 12009 in recurrent malignant gliomas: from preclinical to phase I/II studies. Oligonucleotides 2007;17:201–12.
33. Inman GJ, Nicolás FJ, Callahan JF, Harling JD, Gaster LM, Reith AD, et al. SB-431542 is a potent and specific inhibitor of transforming growth factor-β superfamily type I activin receptor-like kinase (ALK) receptors ALK4, ALK5, and ALK7. Mol Pharmacol 2002;62:65–74.
34. Gadir N, Jackson D, Lee E, Foster D. Defective TGF-β signaling sensitizes human cancer cells to rapamycin. Oncogene 2007;27:1055–62.
35. Filyak Y, Filyak O, Stoika R. Transforming growth factor beta-1 enhances cytotoxic effect of doxorubicin in human lung adenocarcinoma cells of A549 line. Cell Biol Int 2007;31:851–5.
36. Hortobagyi GN, Gomez HL, Li RK, Chung HC, Fein LE, Chan VF, et al. Analysis of overall survival from a phase III study of ixabepilone plus capecitabine versus capecitabine in patients with MBC resistant to anthracyclines and taxanes. Breast Cancer Res Treat 2010;122:409–18.
37. Harper J, Green T, Munroe K, Manning C, Tao J, Simon K, et al. Neutralization of TGFβ enhances the efficacy of chemotherapeutics in a preclinical model of triple negative breast cancer [abstract]. In: Proceedings of the 101st Annual Meeting of the American Association for Cancer Research; 2010 Apr 17–21; Washington, DC. Philadelphia (PA): AACR; Cancer Res 2010;70(8 Suppl): Abstract nr 3826.

Downloaded from mct.aacrjournals.org on November 24, 2015. © 2014 American Association for Cancer Research.

Published OnlineFirst May 9, 2014; DOI: 10.1158/1535-7163.MCT-13-0903

AACR American Association for Cancer Research

Molecular Cancer Therapeutics

EW-7197, a Novel ALK-5 Kinase Inhibitor, Potently Inhibits Breast to Lung Metastasis

Ji Yeon Son, So-Yeon Park, Sol-Ji Kim, et al.

Mol Cancer Ther 2014;13:1704-1716. Published OnlineFirst May 9, 2014.

Updated version	Access the most recent version of this article at: doi:10.1158/1535-7163.MCT-13-0903
Supplementary Material	Access the most recent supplemental material at: http://mct.aacrjournals.org/content/suppl/2014/05/09/1535-7163.MCT-13-0903.DC1.html

Cited articles	This article cites 35 articles, 10 of which you can access for free at: http://mct.aacrjournals.org/content/13/7/1704.full.html#ref-list-1

E-mail alerts	Sign up to receive free email-alerts related to this article or journal.
Reprints and Subscriptions	To order reprints of this article or to subscribe to the journal, contact the AACR Publications Department at pubs@aacr.org.
Permissions	To request permission to re-use all or part of this article, contact the AACR Publications Department at permissions@aacr.org.

Downloaded from mct.aacrjournals.org on November 24, 2015. © 2014 American Association for Cancer Research.